The Journal of Neuroscience, December 15, 2002, 22(24):10593–10602

# Timing and Efficacy of $Ca^{2+}$ Channel Activation in Hippocampal Mossy Fiber Boutons

**Josef Bischofberger, Jörg R. P. Geiger, and Peter Jonas**

*Physiologisches Institut, Universität Freiburg, D-79104 Freiburg, Germany*

The presynaptic $Ca^{2+}$ signal is a key determinant of transmitter release at chemical synapses. In cortical synaptic terminals, however, little is known about the kinetic properties of the presynaptic $Ca^{2+}$ channels. To investigate the timing and magnitude of the presynaptic $Ca^{2+}$ inflow, we performed whole-cell patch-clamp recordings from mossy fiber boutons (MFBs) in rat hippocampus. MFBs showed large high-voltage-activated $Ca^{2+}$ currents, with a maximal amplitude of ~100 pA at a membrane potential of 0 mV. Both activation and deactivation were fast, with time constants in the submillisecond range at a temperature of ~23°C. An MFB action potential (AP) applied as a voltage-clamp command evoked a transient $Ca^{2+}$ current with an average amplitude of ~170 pA and a half-duration of 580 μsec. A prepulse to +40 mV had only minimal effects on the AP-evoked $Ca^{2+}$ current, indicating that presynaptic APs open the voltage-gated $Ca^{2+}$ channels very effectively. On the basis of the experimental data, we developed a kinetic model with four closed states and one open state, linked by voltage-dependent rate constants. Simulations of the $Ca^{2+}$ current could reproduce the experimental data, including the large amplitude and rapid time course of the current evoked by MFB APs. Furthermore, the simulations indicate that the shape of the presynaptic AP and the gating kinetics of the $Ca^{2+}$ channels are tuned to produce a maximal $Ca^{2+}$ influx during a minimal period of time. The precise timing and high efficacy of $Ca^{2+}$ channel activation at this cortical glutamatergic synapse may be important for synchronous transmitter release and temporal information processing.

*Key words: mossy fiber boutons; presynaptic $Ca^{2+}$ inflow; presynaptic $Ca^{2+}$ channels; hippocampus; kinetic model; glutamatergic synapse*

The mossy fiber synapse on CA3 pyramidal neurons is a key synapse that mediates information flow in the trisynaptic circuit of the hippocampus (Jonas et al., 1993; Jung and McNaughton, 1993; Lisman, 1999; Henze et al., 2000). Glutamate release at this synapse is initiated by a complex series of events. These include the invasion of the action potential (AP) into the presynaptic terminal (Geiger and Jonas, 2000), the activation of presynaptic P/Q-, N-, and R-type $Ca^{2+}$ channels (Castillo et al., 1994; Gasparini et al., 2001), and the inflow of $Ca^{2+}$ ions into the presynaptic terminal. The presynaptic $Ca^{2+}$ inflow finally triggers the fusion of synaptic vesicles but also contributes to the regulation of synaptic strength (Salin et al., 1996; Tong et al., 1996; Sabatini and Regehr, 1999).

The spatiotemporal profile of the presynaptic $Ca^{2+}$ transient is of critical importance for the efficacy, timing, and regulation of transmitter release at the mossy fiber synapse. A brief, local transient may trigger fast and highly synchronized glutamate release (Brown and Johnston, 1983; Jonas et al., 1993). In contrast, a more long-lasting, global $Ca^{2+}$ increase is necessary to evoke the release of peptides, e.g., dynorphin (Verhage et al., 1991; Derrick and Martinez, 1996; Williams and Johnston, 1996). Finally, changes in synaptic strength, such as facilitation, post-tetanic potentiation, and long-term potentiation, are thought to be primarily determined by the residual $Ca^{2+}$ (Salin et al., 1996). Short-term plasticity is completely suppressed by the slow exogenous $Ca^{2+}$ buffer EGTA, whereas fast transmitter release is only partly reduced (Salin et al., 1996). This suggests that $Ca^{2+}$ sensors for release and plasticity sense $Ca^{2+}$ signals with different spatiotemporal profiles.

The shape and duration of the presynaptic $Ca^{2+}$ signal is determined by several molecular and structural properties of the presynaptic element, including the duration of the spike, the number of $Ca^{2+}$ channels per release site, the gating properties of the presynaptic channels, and the concentration of endogenous $Ca^{2+}$ buffers (Neher, 1998). The calyx of Held is the only mammalian synapse in which these factors have been determined systematically (Forsythe, 1994; Borst and Sakmann, 1996). In cortical glutamatergic synapses, however, these properties are unknown.

To directly examine the presynaptic $Ca^{2+}$ channels at a cortical glutamatergic synapse, we made patch-clamp recordings from hippocampal mossy fiber boutons (MFBs) in acute brain slices (Geiger and Jonas, 2000; Geiger et al., 2002). We investigated the time course of presynaptic $Ca^{2+}$ inflow and the gating properties of the presynaptic $Ca^{2+}$ channels using whole-cell voltage-clamp recordings. Our approach revealed several fundamental functional parameters of synaptic transmission at the mossy fiber synapse, such as the proportion of $Ca^{2+}$ channels that open during a presynaptic AP and the number of $Ca^{2+}$ ions entering per spike.

Part of the results have been published previously in abstract form (Bischofberger et al., 2001).

## MATERIALS AND METHODS

*Slice preparation*. Transverse 300-μm-thick slices were cut from the hippocampus of 20- to 26-d-old Wistar rats with a custom-built (Geiger et al., 2002) or a commercially available Vibratome (DTK-1000, Dosaka,

Received June 14, 2002; revised Sept. 19, 2002; accepted Sept. 30, 2002.

J.B. was supported by grants from the Deutsche Forschungsgemeinschaft (Bi 642/1-2 and SFB 505/C9). We thank Dr. U. Kraushaar, Dr. S. Hefft, and C. Schmidt-Hieber for critically reading this manuscript, F. Heyde for secretarial help, and A. Blomenkamp and K. Winterhalter for technical assistance.

Correspondence should be addressed to Dr. Josef Bischofberger, Physiologisches Institut, Universität Freiburg, Hermann-Herder-Strasse 7, D-79104 Freiburg, Germany. E-mail: Josef.Bischofberger@physiologie.uni-freiburg.de.

Japan). The animals were killed by decapitation, in accordance with national and institutional guidelines. Slices were kept at 35°C for 30 min after slicing and then at room temperature. For the dissection and storage of slices, we used a saline containing (in mM): 64 NaCl, 25 $NaHCO_3$, 10 glucose, 120 sucrose, 2.5 KCl, 1.25 $NaH_2PO_4$, 0.5 $CaCl_2$, and 7 $MgCl_2$. For the experiments, the slices were transferred into a recording chamber and superfused with a physiological extracellular solution containing (in mM): 125 NaCl, 25 $NaHCO_3$, 25 glucose, 2.5 KCl, 1.25 $NaH_2PO_4$, 2 $CaCl_2$, and 1 $MgCl_2$ (equilibrated with 95% $O_2$/5% $CO_2$ gas mixture).

*Electrophysiology*. Mossy fiber boutons in stratum lucidum of the hippocampal CA3 region were visually identified by their size and location (3–4 μm apparent diameter) (see Fig. 1*A*) (Geiger and Jonas, 2000) using infrared differential interference contrast videomicroscopy (Stuart et al., 1993). Identification was confirmed by the small capacitance (~1 pF whole-cell capacitance readout of the amplifier) and the high input resistance (>1 GΩ). A subset of boutons was filled with biocytin for 30 min in the whole-cell recording configuration. Slices were fixed in 4% paraformaldehyde, stained with Fluorescein Avidin D (Vector Laboratories, Burlingame, CA), and embedded with ProLong Antifade (Molecular Probes, Eugene, OR). Images were taken using a confocal laser scanning microscope (LSM 510, Zeiss, Göttingen, Germany) (see Fig. 1*A*).

Patch pipettes were pulled from borosilicate glass tubing (2.0 mm outer diameter, 0.7 mm wall thickness; Hilgenberg, Malsfeld, Germany). A modified Axopatch 200A amplifier (Axon Instruments, Foster City, CA) was used for current-clamp (I-Clamp fast) and voltage-clamp recording. The amplifier included a bridge-balance circuit for compensation of series resistance in the current-clamp mode, similar to that available in the Axopatch 200B. Current and voltage signals were filtered at 5 and 10 kHz, respectively, with a four-pole low-pass Bessel filter and stored online using a CED 1401plus interface (Cambridge Electronic Design, Cambridge, UK) connected to a personal computer. The sampling frequency was two to four times the filter frequency. Pulses were generated using commercial (CED) or self-made (P. Jonas) programs; the latter allowed us to apply previously recorded APs as voltage-clamp commands.

For whole-cell current-clamp recordings, we used 7–10 MΩ patch pipettes filled with internal solution containing (in mM): 150 $KMeSO_4$, 0.2 EGTA, 2 $MgCl_2$, 2 $Na_2ATP$, 0.3 NaGTP, and 10 HEPES (the pH was adjusted to 7.3 with KOH). Bridge balance was used to compensate the series resistance. In addition, capacitance compensation was used to decrease the charging time of the pipette to <50 μsec. Resting potentials were between −65 and −80 mV. Membrane potentials were set to −80 mV by applying a small hyperpolarizing holding current if necessary. Stimulation of the mossy fiber tract was made with a patch pipette located in the stratum lucidum in subregion CA3c. A stimulus isolation unit (List, Darmstadt, Germany) was used to generate pulses with a duration of 200 μsec and amplitude of −5 to −10 V.

For whole-cell voltage-clamp recordings, we used 5–7 MΩ pipettes filled with a solution containing (in mM): 135 CsCl, 10 EGTA, 4 $MgCl_2$, 4 $Na_2ATP$, 0.3 NaGTP, 10 $Na_2$-phosphocreatine, and 10 HEPES (the pH was adjusted to 7.3 with CsOH). The bath solution contained (in mM): 105 NaCl, 25 $NaHCO_3$, 25 glucose, 2.5 KCl, 1.25 $NaH_2PO_4$, 2 $CaCl_2$, 1 $MgCl_2$, 1 μM tetrodotoxin, 20 tetraethylammonium chloride, and 5 4-aminopyridine to block voltage-gated $Na^+$ and $K^+$ channels, respectively. Leak and capacitive currents were subtracted using two P/−4 sequences within each protocol. Current traces shown in the figures represent the averages of two to five sweeps. Series resistance compensation was enabled in all experiments (compensation 80–90%; lag 20–30 μsec).

The series resistance was typically between 20 and 50 MΩ. Assuming a membrane capacitance of ~1 pF (Geiger and Jonas, 2000), this would correspond to a voltage-clamp time constant $\tau = R_s C_m$ of 20–50 μsec. If the series resistance exceeded a value of 50 MΩ, the recordings were aborted. In some recordings, unclamped tail currents with very slow time course were apparent (these currents may have been generated in neighboring boutons). These recordings were discarded. All chemicals were obtained from Sigma (St. Louis, MO), Merck (Darmstadt, Germany), Riedel-de Haën, or Gerbu. Recordings were made at 23 ± 1°C.

*Data analysis*. The activation time course of the $Ca^{2+}$ current was fitted with a monoexponential function with delayed onset:

$$I(t) = I_0(1 - \exp[-(t - \delta)/\tau]) \text{ for } t \geq \delta, \quad (1)$$

where $I_0$ is the amplitude, $\tau$ is the activation time constant, and $\delta$ is the delay of $Ca^{2+}$ channel activation. To account for the small delay introduced by the lag of series resistance compensation (20–30 μsec) and by electronic filtering (mostly at 5 kHz), the current trace was shifted in time by 100 μsec; with this shift, the end of the rectangular current pulse corresponded to the time when the tail current rose to ~50% of its peak amplitude. The time course of deactivation was fitted with a monoexponential function starting from 50–100 μsec after the peak of the tail currents to minimize contamination by residual capacitive artifacts. The number of $Ca^{2+}$ ions was calculated from the total charge $q$ as $n = q\,N_A/z\,F$ with the Avogadro number $N_A = 6.02\,10^{23}$/mol, the Faraday constant $F$ = 96,485 C/mol, and z = 2. Time course fitting was performed using programs written in Pascal (P. Jonas) based on a modified Gauss–Newton algorithm.

The steady-state activation curve was fitted with a Boltzmann function of the form $f(V) = 1/(1 + \exp[(V_{half} - V)/V_{slope}])$ with $V_{half} = -3.9$ mV and $V_{slope} = 7.1$ mV as best-fit parameters. The values for $V_{half}$ and $V_{slope}$ were then used to fit the *I–V* relationship with a modified Goldman–Hodgkin–Katz equation of the form:

$$I(V) = PV([D - \exp(-V/C)]/[1 - \exp(V/C)])^* f(V), \quad (2)$$

with the voltage $V$, an amplitude factor $P$, a steepness factor $C$, and a parameter $D$ determining current rectification and reversal potential (Sala, 1991). The best-fit parameters were $P = -3.003$ pA/mV, $C = 80.36$ mV, and $D = 0.3933$. The voltage dependence of activation time constants was fitted with the function:

$$\tau(V) = 1/[k_1^* \exp(V/V_1) + k_2^* \exp(-V/V_2)], \quad (3)$$

where $k_1$ are $k_2$ are coefficients and $V_1$ and $V_2$ are steepness factors. The voltage dependence of current amplitudes and time constants was fitted using Prism 3.0 (GraphPad, San Diego, CA).

Amplitude and duration at half-maximal amplitude of APs were measured from baseline potential. Membrane potentials are given without correction for liquid junction potentials. The values indicate mean ± SEM. The error bars also represent SEM. The significance of differences was assessed by a two-tailed Wilcoxon–Mann–Whitney test (Prism 3.0) at the significance level ($P$) indicated.

*Modeling*. The simulations were performed with Mathematica 4.0 (Wolfram Research, Champaign, IL). A set of linear differential equations was defined for a kinetic model with four closed and one open state with voltage-dependent microscopic rate constants for the forward [$\alpha_i(V)$] and backward [$\beta_i(V)$] transitions. The differential equations were defined using the Q-matrix approach of Colquhoun and Hawkes (1977) and numerically solved using Mathematica's NDSolve routine. The analysis of simulated data was identical to that of experimental data; the simulated activation and deactivation time course of the open state were fitted with a monoexponential function with delayed onset and an exponential decay, respectively. The values for activation $\tau$, delay, deactivation $\tau$, and steady-state activation were compared with experimental data by calculating the total sum of the squares of the differences. This sum was minimized by using the FindMinimum routine of Mathematica.

The microscopic rate constants were exponentially dependent on voltage as described by the equations:

$$\alpha_i(V) = \alpha_{io}\exp(V/V_i) \text{ and } \beta_i(V) = \beta_{io}\exp(-V/V_i), \quad (4)$$

with the best-fit parameters $\alpha_{1o} = 4.04$ msec$^{-1}$, $\beta_{1o} = 2.88$ msec$^{-1}$, $V_1 = 49.14$ mV, $\alpha_{2o} = 6.70$ msec$^{-1}$, $\beta_{2o} = 6.30$ msec$^{-1}$, $V_2 = 42.08$ mV, $\alpha_{3o} = 4.39$ msec$^{-1}$, $\beta_{3o} = 8.16$ msec$^{-1}$, $V_3 = 55.31$ mV, $\alpha_{4o} = 17.33$ msec$^{-1}$, $\beta_{4o} = 1.84$ msec$^{-1}$, and $V_4 = 26.55$ mV.

## RESULTS

Whole-cell recordings were made from MFBs in acute rat hippocampal slices (Fig. 1). MFBs were identified by their small size, their small capacitance (~1 pF), and their high input resistance (>1 GΩ) (Geiger and Jonas, 2000). A subset of the boutons was filled with biocytin and stained with Fluorescein Avidin D. Figure 1*A* shows a confocal image of a biocytin-filled MFB, which illustrates the staining of the parent axon and an adjacent MFB. The image also shows filopodial extensions originating from the boutons, which are highly characteristic structural properties of mossy fiber terminals (Acsády et al., 1998).

The presynaptic AP is the primary event that activates presynaptic $Ca^{2+}$ channels and thereby triggers transmitter release. Similar to other presynaptic elements (Borst and Sakmann, 1996;

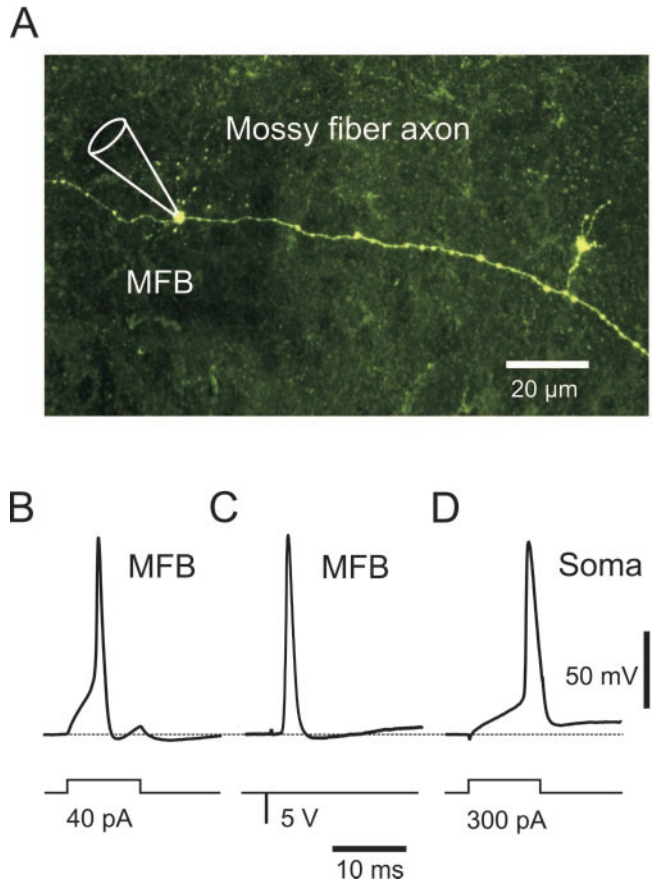


*Figure 1.* Rapid time course of locally evoked and orthodromically propagated APs in MFBs. *A*, Confocal image of an MFB filled with biocytin during the recording and stained with fluorescein avidin D after fixation. Note that the axon runs through the stratum lucidum parallel to the CA3 pyramidal cell layer. *B*, Current-clamp recording from an MFB in whole-cell recording configuration. A small current injection (40 pA, 10 msec) reliably evoked an AP with large amplitude and rapid time course. *C*, Current-clamp recording of an AP evoked by extracellular stimulation of the mossy fiber tract. *D*, AP recorded from a granule cell soma.

Sabatini and Regehr, 1996; Bischofberger and Jonas, 1997), the MFBs were shown to have APs with very rapid time course (Geiger and Jonas, 2000). Figure 1*B* shows a current-clamp recording from an MFB. A small current injection of 20–40 pA evoked an AP with an amplitude of 122.9 ± 2.4 mV and a half-duration of 915 ± 44 μsec (range, 540–1140 μsec; $n = 13$). Similarly, APs could be evoked by extracellular stimulation of the mossy fiber tract (Fig. 1*C*). The amplitude (122.8 ± 2.7 mV) and half-duration (852 ± 62 μsec; $n = 6$) of the AP evoked by remote stimulation were not significantly different from those evoked by direct current injection ($p > 0.4$). In contrast, the half-duration of APs recorded from granule cell somata was much longer, as shown in Figure 1*D* (2.06 ± 0.09 msec; $n = 9$; $p < 0.01$). Thus both locally evoked and orthodromically propagated APs in MFBs showed a fast time course that was significantly faster than APs in granule cell somata.

### MFB $Ca^{2+}$ channels have steep voltage dependence and rapid activation kinetics

To determine the proportion of $Ca^{2+}$ channels opened by the fast presynaptic AP waveform, we analyzed the gating properties of the presynaptic $Ca^{2+}$ channels in MFBs (Figs. 2–4). Figure 2*A* shows whole-cell voltage-clamp recordings of pharmacologically

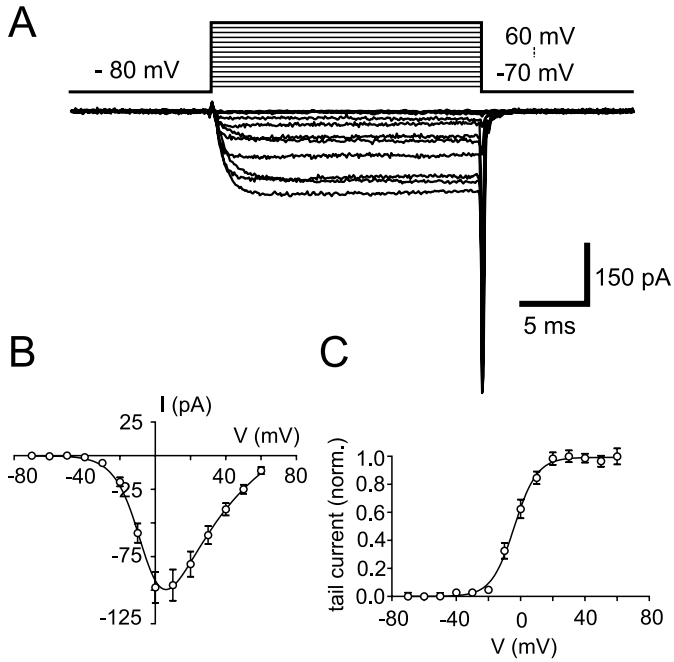


*Figure 2.* Presynaptic voltage-gated $Ca^{2+}$ currents in MFBs. *A*, Voltage-clamp recording of $Ca^{2+}$ currents evoked by 20 msec voltage pulses from a holding potential of −80 mV to potentials of −70 to 60 mV in an MFB. *B*, The maximal current amplitude during the pulses is plotted against pulse potential ($n = 16$) and fitted with Equation 2 (*continuous line*; see Materials and Methods). *C*, To obtain the steady-state activation curve, tail current integrals were plotted against the amplitude of the preceding pulse (5 msec duration). Data were normalized to the maximal value in each experiment, averaged across experiments, and then normalized to the maximal average value ($n = 6$). The activation curve was fitted with a Boltzmann function (*continuous line*). *norm.*, Normalized.

isolated $Ca^{2+}$ currents evoked by 20 msec voltage steps from −70 mV to +60 mV, and Figure 2*B* illustrates the corresponding current–voltage (*I–V*) relationship. The $Ca^{2+}$ currents were activated above −40 mV and reached a maximal current amplitude of 98 ± 11 pA at 0 mV ($n = 16$). At more positive potentials the inward currents decreased, resulting from a reduction in the driving force (Augustine et al., 1985; Borst and Sakmann, 1998).

To obtain the steady-state activation curve, we plotted the integral of the tail currents against the voltage of the preceding pulse (Fig. 2*C*). Because the tail currents were measured at the same potential, the integral gives a precise measure of the number of channels open at the end of the preceding pulse. The steady-state activation data were adequately fitted by a Boltzmann function with a slope factor of 7.1 mV and a midpoint potential of −3.9 mV. We then fitted the bell-shaped *I–V* relation in Figure 2*B* with the product of a Boltzmann function representing channel activation and a modified Goldman–Hodgkin–Katz equation describing the driving force for ion flow (Sala, 1991). The parameters of the Boltzmann function were constrained to the previously determined values. From the fitted curve, the extrapolated reversal potential was determined to be 75.0 mV (Fig. 2*B*). In conclusion, presynaptic $Ca^{2+}$ channels in MFBs show a high activation threshold and a steep voltage dependence.

We next examined the activation and deactivation kinetics of presynaptic $Ca^{2+}$ channels. The time course of activation could be well fitted by a monoexponential function with delayed onset relative to the onset of the pulse (Fig. 3*A*,*B*). The activation time

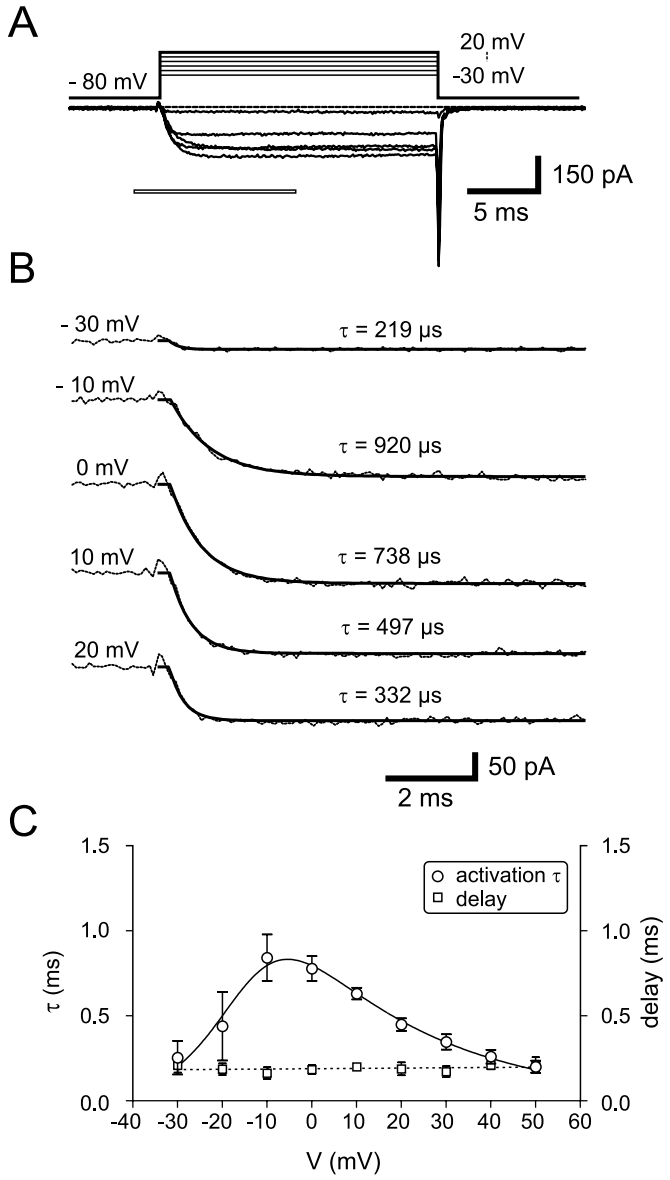


*Figure 3.* MFB $Ca^{2+}$ currents show fast voltage-dependent activation kinetics. *A*, $Ca^{2+}$ currents evoked by rectangular voltage pulses from −30 to 50 mV were analyzed. The part indicated by the *horizontal bar* is shown in *B* at an expanded time scale. *B*, The activation of the $Ca^{2+}$ currents could be well fitted by a monoexponential function with a short delay relative to the onset of the pulse (*thick superimposed lines*). *C*, The activation time constant $\tau$ (○) and the delay (□) are plotted against voltage ($n = 6$). The voltage dependence of the activation $\tau$ was fitted with Equation 3 (*continuous line*). The voltage dependence of the delay was fitted by linear regression (*dashed line*).

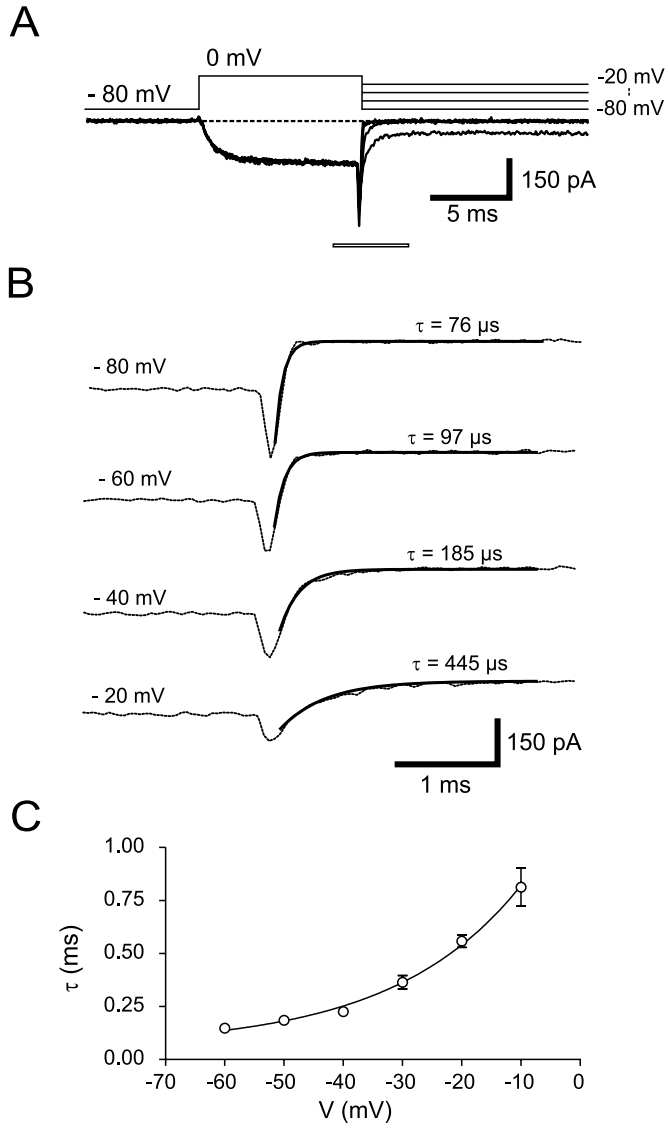


*Figure 4.* MFB $Ca^{2+}$ currents show fast voltage-dependent deactivation kinetics. *A*, A voltage pulse to 0 mV was used to activate the $Ca^{2+}$ channels. The deactivation time course was analyzed after the membrane potential was stepped back to different potentials. The part indicated by the *horizontal bar* is shown in *B* at an expanded time scale. *B*, The deactivation time course could be well fitted with a monoexponential function (*thick superimposed lines*). *C,* The deactivation time constant $\tau$ is plotted against voltage ($n = 6$; same MFBs as in Fig. 3). The voltage dependence of the deactivation $\tau$ was fitted by a monoexponential function (*continuous curve*).

constant $\tau$ and the delay are plotted in Figure 3*C* as a function of voltage. The activation $\tau$ was fast and voltage dependent, ranging from $\tau = 842 \pm 137$ µsec at −10 mV to $201 \pm 35$ µsec at 50 mV ($n = 6$). The voltage dependence could be fitted by Equation 3 with coefficients $k_1 = 1.12$ msec$^{-1}$ and $k_2 = 0.14$ msec$^{-1}$ as well as slope factors $V_1 = 31.5$ mV and $V_2 = 8.6$ mV. In contrast, the delay was independent of voltage, with a mean value of ~200 µsec. Linear regression revealed that the slope of the fitted line was not significantly different from 0 ($p > 0.4$).

Because the amount of $Ca^{2+}$ inflow depends on how long the channels remain open during the presynaptic AP, we further analyzed the deactivation kinetics after a voltage step from 0 mV to negative potentials (−10 mV to −60 mV) (Fig. 4*A*). As shown in Figure 4*B*, the deactivation could be adequately fitted by a monoexponential function. The deactivation $\tau$ was fast, ranging from $813 \pm 90$ µsec at −10 mV to $148 \pm 11$ µsec at −60 mV ($n = 6$). The voltage dependence could be described with an exponential function with an *e*-fold change per 15.0 mV (Fig. 4*C*). Thus both activation and deactivation time constants were fast and highly voltage dependent.

## Presynaptic $Ca^{2+}$ channels are effectively opened by MFB APs

To study the presynaptic $Ca^{2+}$ inflow during natural stimuli, we used previously recorded AP waveforms as voltage-clamp com-

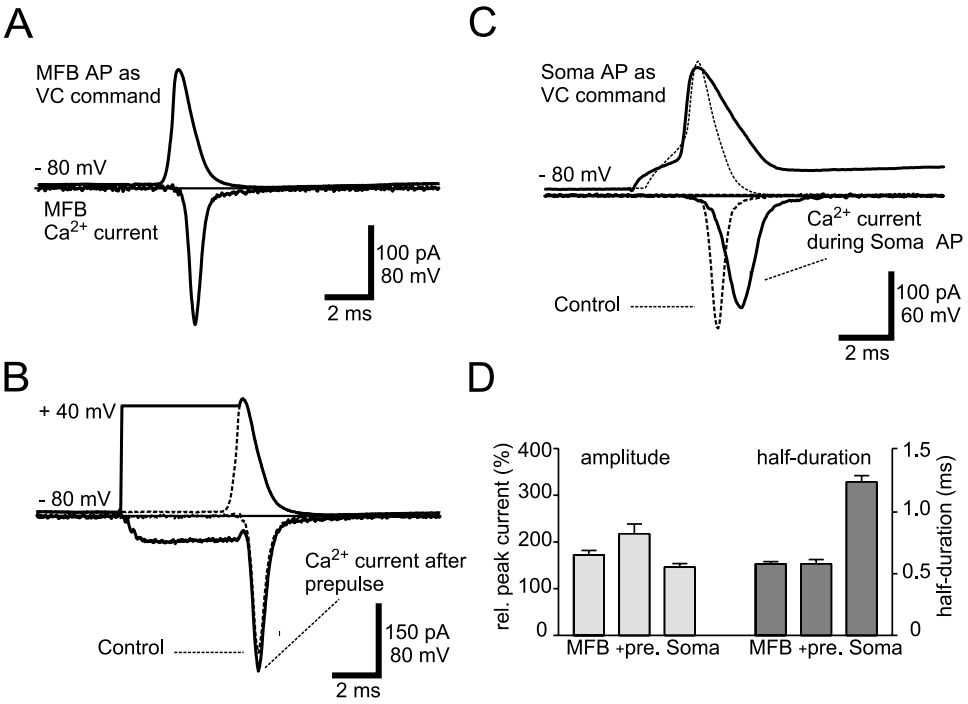


*Figure 5.* Rapid and effective activation of $Ca^{2+}$ currents during AP waveforms. *A*, An AP waveform applied as a voltage-clamp command (*top trace*) instead of a rectangular voltage pulse evoked a transient $Ca^{2+}$ inward current in an MFB (*bottom trace*). The orthodromically propagated AP was previously recorded from a different MFB. *B*, For a 5 msec prepulse period the command voltage was digitally set to +40 mV, which evoked a slightly larger $Ca^{2+}$ peak current (*continuous line*) as compared with control (*dashed line*). *C*, An AP recorded from an MFB (*dashed line*) and a much slower somatic AP waveform (*continuous line*) evoked $Ca^{2+}$ currents with different amplitudes and time courses (*bottom traces*). Both somatic and MFB AP were evoked by direct current injection. *D*, The amplitude and half-duration of currents evoked by different AP waveforms are shown. The peak current was normalized to the maximal current amplitude of the *I–V* relationship (at 0 mV) in the same boutons (corresponding to 100%). The *bar graph* summarizes data from MFB AP experiments ($n = 24$), prepulse experiments (2–5 msec; $n = 9$), and soma AP experiments ($n = 5$); in all cases the waveforms were applied to MFBs.

mands (Scroggs and Fox, 1992) (Fig. 5). A propagated AP evoked a large and brief $Ca^{2+}$ inflow starting at the peak of the AP (Fig. 5*A*). During the repolarization phase the current rapidly increased, reaching a peak amplitude of 187 ± 36 pA ($n = 9$). This current was substantially larger (177 ± 17%) than the maximum peak current amplitude during rectangular voltage pulses to 0 mV in the same MFBs (102 ± 16 pA; $p < 0.01$). The half-duration of the AP-evoked $Ca^{2+}$ current was very short (540 ± 12 μsec; $n = 9$), most probably because of the fast deactivation of the channels at negative potentials. Similar results were obtained with a locally evoked AP waveform (Fig. 5*C*, *dashed line*). The relative peak amplitude and half-duration were 175 ± 10% and 590 ± 19 μsec ($n = 18$), very similar to the respective values for the propagated AP. If data with both waveforms were pooled, a peak amplitude of 171 ± 20 pA (corresponding to a relative amplitude of 173 ± 9%), a half-duration of 579 ± 15 μsec, and a total charge of 119 ± 13 fC were obtained ($n = 24$). This corresponds to an inflow of ~370,000 $Ca^{2+}$ ions per single AP.

To estimate the relative open probability ($P_{open}$) of the $Ca^{2+}$ channels during the AP, we added a prepulse to +40 mV to the AP waveform (Fig. 5*B*,*D*) (Borst and Sakmann, 1998). According to the steady-state activation curve (Fig. 2*C*), this pulse should activate the $Ca^{2+}$ channels with a maximal $P_{open}$. The peak amplitude of the evoked $Ca^{2+}$ currents, however, was only slightly larger as compared with control (124 ± 3% of control; $p < 0.01$; $n = 9$). This indicates that the presynaptic $Ca^{2+}$ channels are opened very effectively by the AP waveform and that the peak $P_{open}$ with a natural stimulus reaches ~80% of the maximal value.

To further elucidate the relation between AP waveform and $Ca^{2+}$ channel activation, we compared the $Ca^{2+}$ current evoked by a fast MFB AP with that evoked by a slow somatic AP waveform (Fig. 5*C*,*D*). The somatic AP evoked a $Ca^{2+}$ current with a half-duration of 1232 ± 51 μsec, significantly larger than that evoked by the brief AP ($p < 0.01$). However, the peak amplitude was reduced (84.6 ± 1.1% of control; $p < 0.01$; $n = 5$). This decrease in peak current amplitude appears to be fundamentally different from the increase in current during AP broadening reported previously for both somatic (Scroggs and Fox, 1992; Wheeler et al., 1996) and presynaptic $Ca^{2+}$ channels (Augustine, 1990; Sabatini and Regehr, 1997). In conclusion, the data suggest that MFB $Ca^{2+}$ channels are effectively opened by the presynaptic APs. To understand the complex dynamic process of activation and deactivation during AP waveforms, we developed a computational model of $Ca^{2+}$ channel gating.

## $Ca^{2+}$ channel gating in MFBs can be described by a five-state kinetic model

The pore-forming $\alpha_1$ subunit of voltage-gated $Ca^{2+}$ channels consists of four domains, each having a positively charged S4 segment, which is believed to be involved in the voltage-dependent gating of the channels (Hille, 2001). Therefore, a model with four voltage-dependent transitions between four closed states and one open state was used (Fig. 6*A*). The microscopic rate constants $\alpha_i$ and $\beta_i$ were assumed to be exponentially dependent on voltage (Eq. 4) (Fig. 6*B*). For a given parameter set, the occupancy of the open state during rectangular voltage pulses was simulated, and the resulting traces were fitted with exponential functions, similar to the experimental data. The parameters for the rate constants $\alpha_i$ and $\beta_i$ were changed until the best approximation of the experimental values for activation $\tau$, delay, deactivation $\tau$, and steady-state activation were achieved. Figure 6, *C* and *D*, shows a comparison of the experimental data with the predictions of the final model (*continuous lines*). In the final set of rate constants, the last transition shows the steepest voltage dependence ($V_i$ = 49, 42, 55, and 27 mV), suggesting cooperativity in channel gating (Fig. 6*B*) (see also Materials and Methods).

We then simulated the $Ca^{2+}$ inflow during APs, using the established model of $Ca^{2+}$ channel gating and the driving force from the *I–V* relation fitted with Equation 2 (Fig. 7). If the brief MFB AP was applied as a voltage command, the simulated $Ca^{2+}$ current had a peak amplitude of 161 pA and a half-duration of

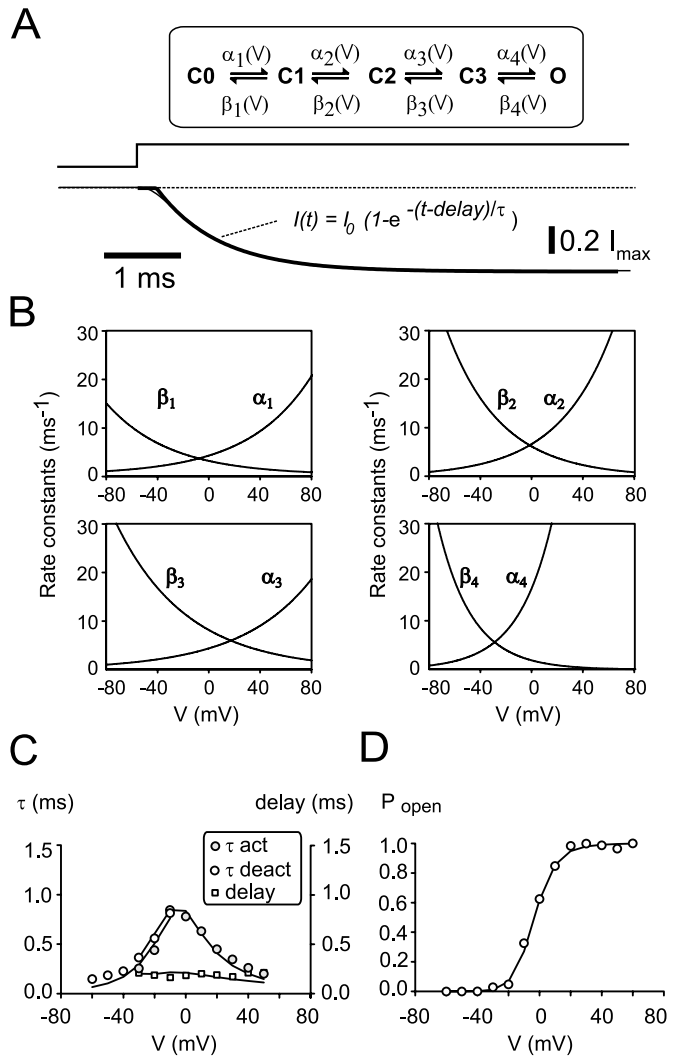


*Figure 6.* A kinetic model of $Ca^{2+}$ channel gating in MFBs. *A*, A serial model with four closed states and one open state was developed (*top panel*). The occupancy of the open state was simulated (*bottom panel*), and the resulting traces were fitted with a monoexponential function with delayed onset, in the same way as the experimental data. $I_{max}$ is the current corresponding to an open probability of 1. Pulse from −80 to 0 mV. *B*, The microscopic rate constants for the transitions $\alpha_i(V)$ and $\beta_i(V)$ as calculated according to Equation 4, using the best-fit parameters given in Materials and Methods. Note the different steepness of the voltage dependence of the rates. *C*, Comparison of measured activation $\tau$ (*filled circles*), deactivation $\tau$ (*open circles*), and delay (*squares*) with the values predicted by the model (*continuous lines*). *D*, Comparison of the measured steady-state activation (*filled circles*) with the steady-state activation curve of the model (*continuous line*).

596 μsec. The peak amplitude corresponded to 176% of the current amplitude during a rectangular voltage pulse to 0 mV, very similar to the experimental data (relative current amplitude 173%; half-duration 579 μsec) (Fig. 5). As shown in Figure 7*A*, the channels started to open during the rising phase of the AP and reached an open probability of 51% at the peak of the AP. The maximal open probability occurred during the early repolarization phase at a potential of 15 mV ($P_{open}$ = 90%). The peak $Ca^{2+}$ inward current occurred slightly later, at a potential of −20 mV ($P_{open}$ = 68%). Subsequently, the channels closed very rapidly and deactivated before complete repolarization to the resting potential. Consistent with the effective opening of the $Ca^{2+}$ channels during the MFB AP, the peak current amplitude was only slightly increased by a 5 msec prepulse to 40 mV (Fig. 7*B*).

To examine the mechanisms underlying the reduction in peak amplitude of the $Ca^{2+}$ current during the slower somatic AP (Fig. 5*C*), we used simulations to compare $Ca^{2+}$ channel activation by fast and slow APs. Similar to the experimental data, the simulated $Ca^{2+}$ current during a broad somatic AP had a prolonged time course and a reduced amplitude (Fig. 7*C*). The simulation shows that the reduction in peak amplitude is caused by a reduction in driving force at this point (−10 vs −20 mV). By contrast, the open probability of the channels at the peak of the $Ca^{2+}$ current was very similar. Figure 7*D* shows a comparison of the relative peak amplitude and half-duration of simulated $Ca^{2+}$ currents evoked by different waveforms. The simulated values for the MFB AP were in close agreement with experimentally determined values (Fig. 5). The results of experiments and modeling converge toward the conclusion that a brief AP waveform leads to efficient and rapid activation of the $Ca^{2+}$ channels, resulting in a high peak open probability.

## Open probability of presynaptic $Ca^{2+}$ channels is highly sensitive to changes in AP waveform

The shape of the presynaptic AP in MFBs is not constant but regulated in an activity-dependent manner (Geiger and Jonas, 2000). Thus we systematically examined the effects of modified AP waveforms, scaled in amplitude and shape in comparison with the original MFB AP (Fig. 8). Figure 8*A* shows the effect of amplitude scaling on the evoked $Ca^{2+}$ inflow, and Figure 8*B* illustrates plots of peak amplitude and charge as a function of AP amplitude. The simulations show that the control AP waveform (*vertical lines*) is a very effective stimulus, producing a presynaptic $Ca^{2+}$ signal with near-maximal peak amplitude and total charge (89 and 98% of the maximal value, respectively). By contrast, a reduction of the AP amplitude by $Na^+$-channel inactivation during high-frequency activity or steady-state depolarization, for example by presynaptic kainate receptors, will substantially reduce the presynaptic $Ca^{2+}$ inflow (Kamiya and Ozawa, 2000; Schmitz et al., 2000).

Similarly, we modified the half-duration of the AP waveform by slowing the time course of repolarization in comparison with the MFB AP (Fig. 8*C*,*D*). The peak amplitude was exponentially dependent on the half-duration (Fig. 8*D*, *top graph*). In contrast, the total charge could be fitted by linear regression (Fig. 8*D*, *bottom graph*), yielding a slope of 73 fC/msec. Thus the model predicts a total $Ca^{2+}$ inflow of ~77–121 fC for the experimental half-durations ranging from 540 to 1140 μsec. Furthermore, it explains the previous observation that dynamic AP broadening leads to a decrease in peak amplitude but an increase in total charge of presynaptic $Ca^{2+}$ inflow (Geiger and Jonas, 2000).

In conclusion, the simulations show that the natural AP is a highly effective stimulus for the activation of the presynaptic $Ca^{2+}$ channels. Additionally, the $Ca^{2+}$ signal can be regulated via the half-duration of the presynaptic AP waveform.

## $Ca^{2+}$ channel gating is optimal for large $Ca^{2+}$ inflow

Similarly, we examined the effects of alterations in channel gating on the amplitude and charge of $Ca^{2+}$ inflow (Fig. 9). Figure 9*A* shows the effects of slower gating, generated by multiplication of all rates with constant factors in the range 1–0.1, and Figure 9*B* shows the effects of acceleration of gating, using factors in the range 1–10. In all simulations, the natural MFB AP waveform was used as a stimulus. Plots of peak amplitude and total charge

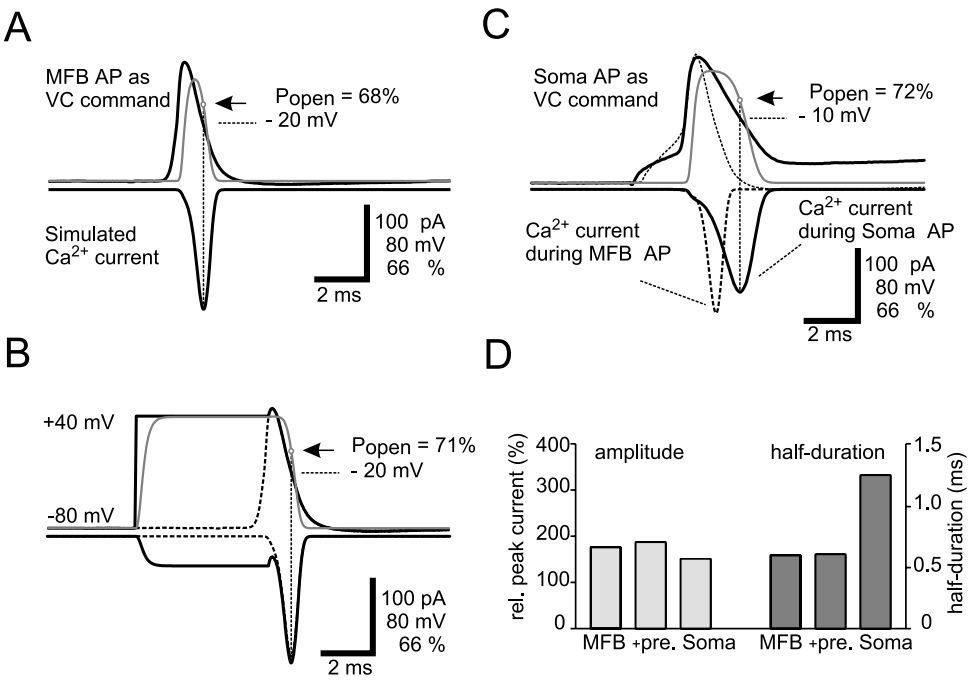


*Figure 7.* High open probability of the model $Ca^{2+}$ channels during AP waveforms. *A*, A propagated MFB AP was used as a voltage command to simulate the activation of the model channels. The calculated open probability (*gray line*) was multiplied by the driving force for $Ca^{2+}$ using Equation 2 to simulate the $Ca^{2+}$ current. *B*, A 5 msec prepulse leads to a slight increase of the $Ca^{2+}$ current (*continuous line*) as compared with control (*dashed line*). *C*, Comparison of the MFB AP (*dashed line*) with a slower somatic AP (*continuous line*). Note that the peak of the $Ca^{2+}$ current occurs at different potentials, as indicated. *D*, Comparison of the relative peak current amplitude and the half-duration during an MFB AP, the prepulse simulation, and the soma AP application (*filled bars*). For the relative peak current, 100% corresponds to the simulated current amplitude during a rectangular voltage pulse to 0 mV.

against the scaling factor indicate that gating kinetics is a critical determinant of the total $Ca^{2+}$ inflow (Fig. 9*C*,*D*). Surprisingly, both slowing down and speeding up the rate constants reduced the $Ca^{2+}$ peak current and the integral. The peak amplitude and total charge produced by the native channels (scaling factor of 1) were 99 and 97% of the maximal values, which were reached with factors slightly below 1. Furthermore, both slowing down and speeding up of the rates lead to prolonged time course of $Ca^{2+}$ inflow. In particular, the acceleration of the rates by a factor of >2 leads to a biphasic $Ca^{2+}$ current, increasing the total time interval during which $Ca^{2+}$ inflow occurs (Fig. 9*B*). In conclusion, these simulations unequivocally show that the gating of presynaptic $Ca^{2+}$ channels in MFBs is optimal for producing a transient $Ca^{2+}$ inflow with maximal amplitude and minimal duration. Whether this conclusion also holds true at physiological temperatures remains to be established. However, because the $Q_{10}$ values for AP duration (~2.2) (Geiger and Jonas, 2000; this paper) and $Ca^{2+}$ channel activation kinetics are similar (~2.5) (Swandulla and Armstrong, 1988), this appears to be very likely.

## DISCUSSION

The present results provide the first description of $Ca^{2+}$ channel gating in a cortical presynaptic terminal. The major finding was that the fast activation kinetics of the channels leads to a high open probability and a remarkably large $Ca^{2+}$ inflow of ~370,000 $Ca^{2+}$ ions during a single AP. The gating of presynaptic $Ca^{2+}$ channels appears to be precisely tuned to achieve a maximal $Ca^{2+}$ influx during a minimal period of time.

### Rapid gating of presynaptic $Ca^{2+}$ channels

The gating of presynaptic $Ca^{2+}$ channels could be adequately described by a serial gating model with four closed states and one open state. In contrast, neither alternative models with two or three closed states nor Hodgkin–Huxley models with an integer number of independent gating particles provided a sufficient description of the data (J. Bischofberger, unpublished data). In the models with two or three closed states, the delay of activation was smaller than that observed experimentally. In Hodgkin–Huxley models, deactivation is faster than activation at the same potential, with a ratio that approaches the number of gating particles (Kay and Wong, 1987; Zidanic and Fuchs, 1995; Mennerick and Matthews, 1998). Thus the functional properties of presynaptic $Ca^{2+}$ channels in MFBs are inconsistent with the assumption of independently moving gating particles.

Our model suggests that the voltage dependence differs among the transition rates. This has to be interpreted as a different movement of the S4 segments, the putative voltage sensors, because the number of positive charges per S4 segment is comparable among domains (approximately five) (Soong et al., 1993). For the first three transitions, the steepness factors range from 42 to 55 mV, which would correspond to an S4 segment movement by 9–12% along the total electric field. In contrast, for the final transition leading to the open state, the steepness factor is 27 mV, which would correspond to an S4 segment movement by 19%. Interdomain differences in voltage-dependent movement of S4 segments were experimentally demonstrated for voltage-dependent $Na^{+}$ channels (Cha et al., 1999). An analogous biophysical approach will reveal whether similar interdomain differences exist in voltage-gated $Ca^{2+}$ channels, as our results would suggest.

### Efficiency and timing of $Ca^{2+}$ channel opening during single APs

The activation kinetics of the presynaptic $Ca^{2+}$ channels in MFBs appear to be much faster than the activation of $Ca^{2+}$ channels in invertebrate presynaptic terminals (Llinás et al., 1981; Wright et al., 1996). For the squid giant synapse it was suggested that the relative open probability of $Ca^{2+}$ channels during a single AP was ~10% (Pumplin et al., 1981; Augustine, 1990), markedly less than the value estimated for the MFB (~90%). The gating is also faster than that described for somatodendritic high-voltage-activated $Ca^{2+}$ channels in CA1 pyramidal neurons (Kay and Wong, 1987). This may be correlated to the slower time course of somatodendritic voltage signals, e.g., synaptic potentials or backpropagating APs (Magee and Johnston, 1995; Normann et al., 2000).

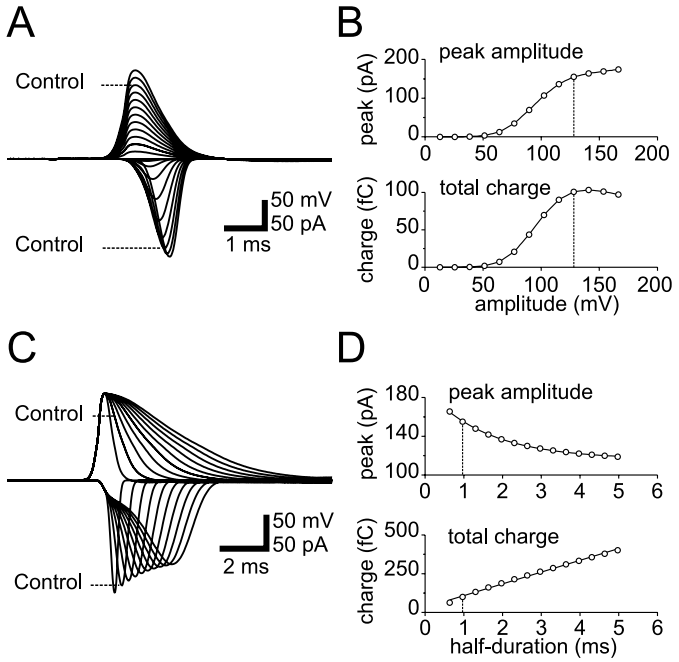


*Figure 8.* Presynaptic $Ca^{2+}$ inflow is highly sensitive to changes in AP amplitude and shape. *A*, The amplitude of the measured MFB AP was scaled from 10 to 120% in 10% steps and used to activate the $Ca^{2+}$ channel model. *B*, The resulting peak amplitude and the total charge were plotted against the AP amplitude. The amplitude of the measured AP is indicated by the *dashed vertical lines*. *C*, The decay phase of the AP waveform was scaled by digitally shrinking or expanding the timescale of the trace after the peak from 50 to 500% in 50% steps. *D*, The resulting peak amplitude and the total charge were plotted against the AP half-duration. The half-duration of the measured AP is indicated by the *dashed vertical lines*. In *B* the data points were connected by *straight lines*, and the *curves* in *D* are fits with an exponential function plus a constant (*top graph*) or linear function (*bottom graph*).

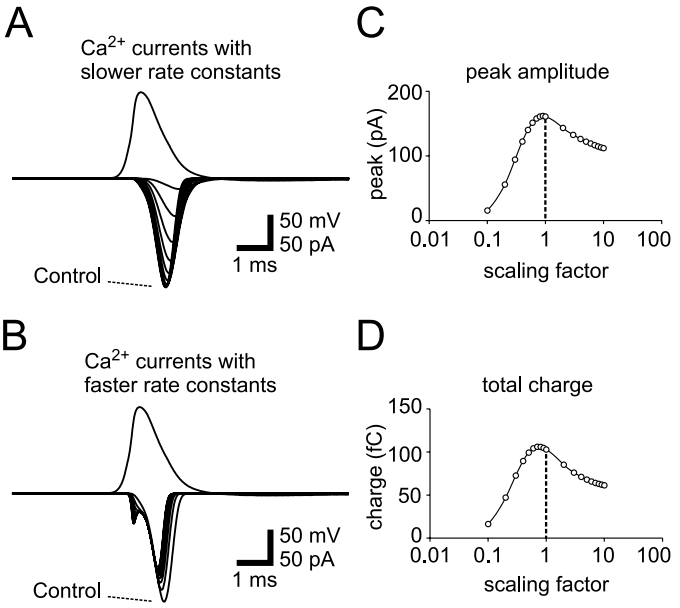


*Figure 9.* Presynaptic $Ca^{2+}$ inflow is highly sensitive to changes in gating kinetics. *A*, All rate constants in the kinetic model were multiplied by a constant factor (1–0.1 in steps of 0.1) to selectively slow channel gating without affecting steady-state activation. Simulated $Ca^{2+}$ currents are shown superimposed. *B*, The gating was accelerated by multiplying rate constants with a constant factor (1–10 in steps of 1). *C*, *D*, Peak amplitude (*C*) and charge (*D*) of the simulated current, plotted against the scaling factor on a logarithmic scale. The properties of the original $Ca^{2+}$ channel are indicated by the *vertical dashed lines*. Curves in *C* and *D* represent cubic spline interpolations.

The activation kinetics of the $Ca^{2+}$ channels in MFBs, however, is similar to that reported for presynaptic $Ca^{2+}$ channels in giant vertebrate synaptic terminals (Zidanic and Fuchs, 1995; Borst and Sakmann, 1998; Mennerick and Matthews, 1998). In the calyx of Held, single APs evoke a $Ca^{2+}$ current with a relative peak open probability of ~70% and an average half-duration of ~400 μsec (24°C) (Borst and Sakmann, 1998), comparable with the values reported here. Thus, although the two types of synapses differ in morphological properties, subunit composition of postsynaptic receptors, and functional role in the neuronal circuit, the efficacy and timing of presynaptic $Ca^{2+}$ inflow appear to be similar (Von Gersdorff and Borst, 2002).

In the MFB, the $Ca^{2+}$ channels open very early during the rising phase of the AP with a relative $P_{open}$ of ~50% at the peak of the AP; however, no substantial current can be detected at this point, because of the small driving force. The $Ca^{2+}$ inflow is restricted to the repolarization phase of the AP (Figs. 5*A*, 7*A*). In contrast, for parallel fiber synapses in the cerebellum, it was reported that rapid $Ca^{2+}$ channel gating leads to substantial $Ca^{2+}$ current during the upstroke and peak of the presynaptic AP (Sabatini and Regehr, 1996, 1997). This situation appears to be very different from that in the MFB because the experimentally determined *I–V* relationship for the $Ca^{2+}$ currents in the MFB is obviously inconsistent with a large driving force at the peak of the AP (at ~45 mV) (Fig. 2*B*). If these discrepancies are not caused by technical difficulties in deriving the voltage and $Ca^{2+}$ current time course from fluorescence signals (Sabatini and Regehr, 1996, 1997), they may suggest a synapse-specific difference in presynaptic ion flow.

## How many $Ca^{2+}$ ions are necessary for transmitter release?

The present results provide quantitative estimates of fundamental parameters of the early presynaptic events that are relevant for both efficacy and timing of synaptic transmission. We found that the average peak amplitude of the presynaptic $Ca^{2+}$ current evoked by a natural AP is 170 pA. With a single-channel current of 0.2 pA at physiological external $Ca^{2+}$ concentrations (Gollasch et al., 1992), this corresponds to 850 $Ca^{2+}$ channels open at the peak in a presynaptic terminal. The total $Ca^{2+}$ inflow evoked by a single AP was 120 fC, corresponding to ~370,000 $Ca^{2+}$ ions per bouton.

MFBs have multiple release sites (up to 37 in an incompletely reconstructed large MFB) (Chicurel and Harris, 1992). Thus the measured presynaptic $Ca^{2+}$ current would approximately correspond to 23 $Ca^{2+}$ channels open at the peak at a single release site, producing an inflow of ~10,000 $Ca^{2+}$ ions per site. Although these are only rough estimates, the results are consistent with previous suggestions at boutons of neocortical pyramidal cells (~40 channels per bouton, ~5500 $Ca^{2+}$ ions) (Koester and Sakmann, 2000) and the calyx of Held (~20 channels per site, ~13000 $Ca^{2+}$ ions) (Borst and Sakmann, 1996; Sätzler et al., 2002). Furthermore, they are consistent with the cooperativity between different types of $Ca^{2+}$ channels in triggering transmitter release at the mossy fiber–CA3 synapse (Castillo et al., 1994) and other cortical glutamatergic synapses (Luebke et al., 1993; Wheeler et al., 1994; Dunlap et al., 1995). Although we cannot

exclude a subpopulation of release sites endowed with a single $Ca^{2+}$ channel (Stanley, 1997), our results suggest that most of the sites are controlled by multiple channels. This may increase the reliability of excitation–secretion coupling in central glutamatergic synapses.

### Functional significance for synaptic transmission at MFB–CA3 pyramidal neuron synapse

The quantitative properties of the presynaptic $Ca^{2+}$ inflow are also critical for the timing of transmitter release. A large $Ca^{2+}$ signal may help to minimize synaptic delay. Transmitter release requires the binding of multiple $Ca^{2+}$ ions to the $Ca^{2+}$ sensor (Augustine, 2001). As shown for the calyx of Held, the sequential binding of multiple $Ca^{2+}$ ions introduces a significant delay between the $Ca^{2+}$ inflow and the transmitter release (Schneggenburger and Neher, 2000). This delay was strongly dependent on the $Ca^{2+}$ concentration. Thus, a large $Ca^{2+}$ signal will provide a rapid onset of neurotransmitter release. Additionally, the fast deactivation of the presynaptic $Ca^{2+}$ channels may be important for the termination of exocytosis. The rapid $Ca^{2+}$ signaling will be a critical determinant of the precise timing of transmitter release at the MFB to CA3–pyramidal cell synapse, where the half-width of the first latency distribution is ~500 μsec (Jonas et al., 1993). Similar rules may apply for synapses formed by the mossy fiber system onto other types of target cells, e.g., at the granule cell to basket cell synapse, formed by mossy fiber collaterals on inhibitory interneurons (Geiger et al., 1997).

The precise timing during single APs may be relevant for the temporal encoding of information in the hippocampus (Lisman, 1999). It was shown that granule cells and pyramidal cells fire APs in a specific temporal relationship to the theta rhythm when the animal passes through the place field of the cell (Jung and McNaughton, 1993; O'Keefe and Recce, 1993). When the animal is in the center of the place field of a given neuron, this neuron fires APs earlier in the theta cycle than neurons with adjacent place fields (Skaggs and McNaughton, 1996; Skaggs et al., 1996). For temporal coding with high fidelity, neurons with the same place field should fire exactly at the same time (Lisman, 1999). Because the mossy fiber tract is the major excitatory pathway that connects the associative network in the dentate gyrus/hilus with that in the CA3 region, the precise timing of presynaptic $Ca^{2+}$ inflow and transmitter release might be important for the correct temporal sequence of place cell firing and, more generally, for the temporal coding of episodic memory.

## REFERENCES


Acsády L, Kamondi A, Sík A, Freund T, Buzsáki G (1998) GABAergic cells are the major postsynaptic targets of mossy fibers in the rat hippocampus. J Neurosci 18:3386–3403.

Augustine GJ (1990) Regulation of transmitter release at the squid giant synapse by presynaptic delayed rectifier potassium current. J Physiol (Lond) 431:343–364.

Augustine GJ (2001) How does calcium trigger neurotransmitter release? Curr Opin Neurobiol 11:320–326.

Augustine GJ, Charlton MP, Smith SJ (1985) Calcium entry into voltage-clamped presynaptic terminals of squid. J Physiol (Lond) 367:143–162.

Bischofberger J, Jonas P (1997) Action potential propagation into the presynaptic dendrites of rat mitral cells. J Physiol (Lond) 504:359–365.

Bischofberger J, Geiger JRP, Jonas P (2001) Presynaptic $Ca^{2+}$ influx into hippocampal mossy fiber boutons. Soc Neurosci Abstr 31:384.6.

Borst JGG, Sakmann B (1996) Calcium influx and transmitter release in a fast CNS synapse. Nature 383:431–434.

Borst JGG, Sakmann B (1998) Calcium current during a single action potential in a large presynaptic terminal of the rat brainstem. J Physiol (Lond) 506:143–157.

Brown TH, Johnston D (1983) Voltage-clamp analysis of mossy fiber synaptic input to hippocampal neurons. J Neurophysiol 50:487–507.

Castillo PE, Weisskopf MG, Nicoll RA (1994) The role of $Ca^{2+}$ channels in hippocampal mossy fiber synaptic transmission and long-term potentiation. Neuron 12:261–269.

Cha A, Ruben PC, George AL, Fujimoto E, Bezanilla F (1999) Voltage sensors in domain III and IV, but not I and II, are immobilized by $Na^{+}$ channel fast inactivation. Neuron 22:73–87.

Chicurel ME, Harris KM (1992) Three-dimensional analysis of the structure and composition of CA3 branched dendritic spines and their synaptic relationships with mossy fiber boutons in the rat hippocampus. J Comp Neurol 325:169–182.

Colquhoun D, Hawkes AG (1977) Relaxation and fluctuations of membrane currents that flow through drug-operated channels. Proc R Soc Lond B Biol Sci 199:231–262.

Derrick BE, Martinez JL (1996) Associative, bidirectional modifications at the hippocampal mossy fibre-CA3 synapse. Nature 381:429–434.

Dunlap K, Luebke JI, Turner TJ (1995) Exocytotic $Ca^{2+}$ channels in mammalian central neurons. Trends Neurosci 18:89–98.

Forsythe ID (1994) Direct patch recording from identified presynaptic terminals mediating glutamatergic EPSCs in the rat CNS, in vitro. J Physiol (Lond) 479:381–387.

Gasparini S, Kasyanov AM, Pietrobon D, Voronin LL, Cherubini E (2001) Presynaptic R-type calcium channels contribute to fast excitatory synaptic transmission in the rat hippocampus. J Neurosci 21:8715–8721.

Geiger JRP, Jonas P (2000) Dynamic control of presynaptic $Ca^{2+}$ inflow by fast-inactivating $K^{+}$ channels in hippocampal mossy fiber boutons. Neuron 28:927–939.

Geiger JRP, Lübke J, Roth A, Frotscher M, Jonas P (1997) Submillisecond AMPA receptor-mediated signaling at a principal neuron-interneuron synapse. Neuron 18:1009–1023.

Geiger JRP, Bischofberger J, Vida I, Fröbe U, Pfitzinger S, Weber HJ, Haverkampf K, Jonas P (2002) Patch-clamp recording in brain slices with improved slicer technology. Pflügers Arch 443:491–501.

Gollasch M, Hescheler J, Quayle JM, Patlak JB, Nelson MT (1992) Single calcium channel currents of arterial smooth muscle at physiological calcium concentrations. Am J Physiol 263:C948–C952.

Henze DA, Urban NN, Barrionuevo G (2000) The multifarious hippocampal mossy fiber pathway: a review. Neuroscience 98:407–427.

Hille B (2001) Ionic channels of excitable membranes, Ed 3. Sunderland, MA: Sinauer.

Jonas P, Major G, Sakmann B (1993) Quantal components of unitary EPSCs at the mossy fiber synapse on CA3 pyramidal cells of rat hippocampus. J Physiol (Lond) 472:615–663.

Jung MW, McNaughton BL (1993) Spatial selectivity of unit activity in the hippocampal granular layer. Hippocampus 3:165–182.

Kamiya H, Ozawa S (2000) Kainate receptor-mediated presynaptic inhibition at the mouse hippocampal mossy fibre synapse. J Physiol (Lond) 523:653–665.

Kay AR, Wong RKS (1987) Calcium current activation kinetics in isolated pyramidal neurones of the CA1 region of the mature guinea-pig hippocampus. J Physiol (Lond) 392:603–616.

Koester HJ, Sakmann B (2000) Calcium dynamics associated with action potentials in single nerve terminals of pyramidal cells in layer 2/3 of the young rat neocortex. J Physiol (Lond) 529:625–646.

Lisman JE (1999) Relating hippocampal circuitry to function: recall of memory sequences by reciprocal dentate-CA3 interactions. Neuron 22:233–242.

Llinás R, Steinberg IZ, Walton K (1981) Presynaptic calcium currents in squid giant synapse. Biophys J 33:289–322.

Luebke JI, Dunlap K, Turner TJ (1993) Multiple calcium channel types control glutamatergic synaptic transmission in the hippocampus. Neuron 11:895–902.

Magee JC, Johnston D (1995) Synaptic activation of voltage-gated channels in the dendrites of hippocampal pyramidal neurons. Science 268:301–304.

Mennerick S, Matthews G (1998) Rapid calcium-current kinetics in synaptic terminals of goldfish retinal bipolar neurons. Vis Neurosci 15:1051–1056.

Neher E (1998) Vesicle pools and $Ca^{2+}$ microdomains: new tools for understanding their roles in neurotransmitter release. Neuron 20:389–399.

Normann C, Peckys D, Schulze CH, Walden J, Jonas P, Bischofberger J (2000) Associative long-term depression in the hippocampus is dependent on postsynaptic N-type $Ca^{2+}$ channels. J Neurosci 20:8290–8297.

O'Keefe J, Recce ML (1993) Phase relationship between hippocampal place units and the EEG theta rhythm. Hippocampus 3:317–330.

Pumplin DW, Reese TS, Llinás R (1981) Are the presynaptic membrane particles the calcium channels? Proc Natl Acad Sci USA 78:7210–7213.

Sabatini BL, Regehr WG (1996) Timing of neurotransmission at fast synapses in the mammalian brain. Nature 384:170–172.

Sabatini BL, Regehr WG (1997) Control of neurotransmitter release by presynaptic waveform at the granule cell to Purkinje cell synapse. J Neurosci 17:3425–3435.

Sabatini BL, Regehr WG (1999) Timing of synaptic transmission. Annu Rev Physiol 61:521–542.

Sala F (1991) Activation kinetics of calcium currents in bullfrog sympathetic neurones. J Physiol (Lond) 437:221–238.
Salin PA, Scanziani M, Malenka RC, Nicoll RA (1996) Distinct short-term plasticity at two excitatory synapses in the hippocampus. Proc Natl Acad Sci USA 93:13304–13309.
Sätzler K, Söhl LF, Bollmann JH, Borst JGG, Frotscher M, Sakmann B, Lübke JHR (2002) Three-dimensional reconstruction of a giant synapse between the calyx of Held and an MNTB principal neuron. J Neurosci, in press.
Schmitz D, Frerking M, Nicoll RA (2000) Synaptic activation of presynaptic kainate receptors on hippocampal mossy fiber synapses. Neuron 27:327–338.
Schneggenburger R, Neher E (2000) Intracellular calcium dependence of transmitter release rates at a fast central synapse. Nature 406:889–893.
Scroggs RS, Fox AP (1992) Multiple $Ca^{2+}$ currents elicited by action potential waveforms in acutely isolated adult rat dorsal root ganglion neurons. J Neurosci 12:1789–1801.
Skaggs WE, McNaughton BL (1996) Replay of neuronal firing sequences in rat hippocampus during sleep following spatial experience. Science 271:1870–1873.
Skaggs WE, McNaughton BL, Wilson MA, Barnes CA (1996) Theta phase precession in hippocampal neuronal populations and the compression of temporal sequences. Hippocampus 6:149–172.
Soong TW, Stea A, Hodson CD, Dubel SJ, Vincent SR, Snutch TP (1993) Structure and functional expression of a member of the low voltage-activated calcium channel family. Science 260:1133–1136.
Stanley EF (1997) The calcium channel and the organization of the presynaptic transmitter release face. Trends Neurosci 20:404–409.
Stuart GJ, Dodt HU, Sakmann B (1993) Patch-clamp recordings from the soma and dendrites of neurons in brain slices using infrared video microscopy. Pflügers Arch 423:511–518.
Swandulla D, Armstrong CM (1988) Fast-deactivating calcium channels in chick sensory neurons. J Gen Physiol 92:197–218.
Tong G, Malenka RC, Nicoll RA (1996) Long-term potentiation in cultures of single hippocampal granule cells: a presynaptic form of plasticity. Neuron 16:1147–1157.
Verhage M, McMahon HT, Ghijsen WE, Boomsma F, Scholten G, Wiegant VM, Nicholls DG (1991) Differential release of amino acids, neuropeptides, and catecholamines from isolated nerve terminals. Neuron 6:517–524.
Von Gersdorff H, Borst JGG (2002) Short-term plasticity at the calyx of Held. Nat Rev Neurosci 3:53–64.
Wheeler DB, Randall A, Tsien RW (1994) Roles of N-type and Q-type $Ca^{2+}$ channels in supporting hippocampal synaptic transmission. Science 264:107–111.
Wheeler DB, Randall A, Tsien RW (1996) Changes in action potential duration alter reliance of excitatory synaptic transmission on multiple types of $Ca^{2+}$ channels in rat hippocampus. J Neurosci 16:2226–2237.
Williams SH, Johnston D (1996) Actions of endogenous opioids on NMDA receptor-independent long-term potentiation in area CA3 of the hippocampus. J Neurosci 16:3652–3660.
Wright SN, Brodwick MS, Bittner GD (1996) Presynaptic calcium currents at voltage clamped excitor and inhibitor nerve terminals of crayfish. J Physiol (Lond) 496:347–361.
Zidanic M, Fuchs PA (1995) Kinetic analysis of barium currents in chick cochlear hair cells. Biophys J 68:1323–1336.